Enhanced mixing via alternating injection in radial Hele-Shaw flows

Ching-Yao Chen,* Yi-Cheng Huang, and Yu-Sheng Huang
Department of Mechanical Engineering, National Chiao Tung University, Hsinchu 30010, Taiwan, Republic of China

José A. Miranda†
Departamento de Física, Universidade Federal de Pernambuco, Recife, Pernambuco 50670-901, Brazil
(Received 6 August 2015; published 7 October 2015)

Mixing at low Reynolds numbers, especially in the framework of confined flows occurring in Hele-Shaw cells, porous media, and microfluidic devices, has attracted considerable attention lately. Under such circumstances, enhanced mixing is limited due to the lack of turbulence, and absence of sizable inertial effects. Recent studies, performed in rectangular Hele-Shaw cells, have demonstrated that the combined action of viscous fluid fingering and alternating injection can dramatically improve mixing efficiency. In this work, we revisit this important fluid mechanical problem, and analyze it in the context of radial Hele-Shaw flows. The development of radial fingering instabilities under alternating injection conditions is investigated by intensive numerical simulations. We focus on the impact of the relevant physical parameters of the problem (Péclet number Pe, viscosity contrast A, and injection time interval Δt) on fluid mixing performance.

DOI: 10.1103/PhysRevE.92.043008 PACS number(s): 47.51.+a, 47.15.gp, 47.20.Gv, 47.54.−r

I. INTRODUCTION

The viscous fingering (or, Saffman-Taylor) instability [1] occurs in both immiscible and miscible fluids, when a less viscous fluid displaces a more viscous one in a porous medium, or in the confined environment of a Hele-Shaw cell [2–4]. Instead of advancing as a uniform front, the fluid-fluid interface develops peculiar structures in the form of fingers. As time progresses, the fingers change in size and shape, which leads to the formation of complex patterns. Experimental and theoretical studies in this system focus on two principal flow geometries: (i) rectangular [1–3] and (ii) radial [5–7]. In rectangular (or, channel) cells the initial unperturbed interface is straight, and the unperturbed flow is uniform and parallel to cell walls. In the radial case, the unperturbed interface is circular with the less viscous fluid pumped into the more viscous one at a point source, and the flow evolves radially outward.

Viscous fluid fingering plays a key role in a number of natural and technological processes, including flows in porous media [2], enhanced oil recovery [8], and microfluidics [9]. Depending on the situation, viscous fingering formation can be an obstacle or a benefit. For example, in oil recovery it is mostly undesirable. In fact, the fingering instability is a major source of poor oil recovery once rapidly evolving injected water fingers may reach the entrance of the well and mainly water, and not the more viscous oil, is regained. This type of important practical difficulty has motivated a number of recent studies that suggest different strategies intended to inhibit the emergence of viscous fingering. One particularly successful controlling technique has been proposed in Refs. [10–14], where proper control of the shape of the emergent fingered patterns has been achieved through the employment of time-dependent injection schemes. In these studies, it has been shown that time manipulation of the injection flow rate of the less viscous fluid can either offer a way to control the number of the uprising fingers, or to simply suppress their appearance.

However, under other physical circumstances or industrial applications, the emergence of intense viscous fingering can be something beneficial. For instance, it has been recently shown that intense fingering destabilization in rectangular Hele-Shaw cells does favor fluid mixing in confined systems, such as in microfluidic devices [15,16]. As these confined fluid systems typically have a small Reynolds number, inertial effects are negligible, and turbulence does not set in. Therefore, achieving enhanced fluid mixing is not really trivial. In a follow-up paper [17], the same group of researchers has demonstrated that confined fluid mixing in rectangular Hele-Shaw cells can be improved further, if one employs an alternating injection protocol. Within this methodology, one fluid is injected followed by another one to lower the unfavorable viscosity ratios between displacing and displaced fluids. In Ref. [17] it has been found that the combined action of alternating injection and viscous fingering actually leads to a dramatic increase in mixing efficiency. It should be noted that previous studies of viscous fingering in alternating injection analyzed the spreading of a single slug in radial [18] and rectangular geometry [19–21]. More recently, a cyclic injection procedure has also been applied to study reactive displacement in porous media flows [22].

Due to the practical and academic relevance of the confined mixing fluid problem studied by Jha *et al.* in Refs. [15–17] for the rectangular Hele-Shaw setup, it is also of interest to understand the emergence of similar phenomena for miscible displacements in radial Hele-Shaw cells. It is worth noting that the radial geometry flow has a close connection to important single-source applications, namely those related to enhanced oil recovery. The major goal of this research is to investigate under what circumstances one can obtain enhanced mixing via alternating injection in radial Hele-Shaw flows. In order to do that, we perform intensive numerical simulations of the system, and examine how alternating injection couples to fingering effects, particularly during fully nonlinear stages of mixing pattern evolution.

*chingyao@mail.nctu.edu.tw
†jme@df.ufpe.br

II. PHYSICAL PROBLEM AND MATHEMATICAL FORMULATION

A. Governing equations

We study a binary system containing two incompressible viscous fluids, which are miscible to each other, in a radial Hele-Shaw cell of constant gap thickness b. The viscosities of the fluids are denoted as η_1 (fluid 1), and η_2 (fluid 2), and we assume that $\eta_2 \geqslant \eta_1$. Initially, the cell is fully occupied by fluid 2. In the framework of the alternating injection procedure, equal amounts of fluid 1 and fluid 2 are injected in sequence. The process continues up to a time $t = t_f$, when the area of the total injected fluid expands to $\pi {D_f}^2/4$ in a stable injection condition without fingering instability. Here D_f denotes the diameter of the resulting circular domain. At first, the diffusive fluid-fluid interface is a small circular core of diameter D_0, and a Cartesian coordinate system (x, y) is defined in such a way that its origin is located at the center of this core region. Consequently, the areal injection rate can be obtained as $Q = \pi({D_f}^2 - {D_0}^2)/4t_f$, in which the total injection duration for both fluid 1 and fluid 2 is $t_f/2$ each. In accordance with the general phenomenology of the Saffman-Taylor problem, since $\eta_2 > \eta_1$, the interface becomes unstable during the injection of the less viscous fluid 1, while it expands in a stable manner under the injection of the more viscous fluid 2.

The evolution of the system in such a confined Hele-Shaw cell geometry is governed by the following set of gap-averaged equations [23]:

$$\nabla \cdot \mathbf{u} = 0, \tag{1}$$

$$\nabla p = -\frac{12\eta}{b^2}\mathbf{u}, \tag{2}$$

$$\frac{\partial c}{\partial t} + \mathbf{u}\cdot\nabla c = D\nabla^2 c. \tag{3}$$

Equation (1) expresses the incompressibility condition, where $\mathbf{u}$ is the two-dimensional velocity vector with components (u_x, u_y). A Darcy's law for miscible Hele-Shaw flows is expressed by Eq. (2) where p is the pressure, and η is the viscosity of the binary system. The concentration equation is given by Eq. (3), where D is the constant diffusion coefficient. In Eq. (3) c represents concentration of the less viscous fluid 1, such that $c = 1$ and $c = 0$ for the less viscous fluid 1, and the more viscous fluid 2, respectively. Viscosity η and concentration c are assumed to be related as [24]

$$\eta(c) = \eta_1 e^{[R(1-c)]}, \quad R = \ln\left(\frac{\eta_2}{\eta_1}\right). \tag{4}$$

In order to render the governing equations and relevant variables dimensionless, D_f and t_f are taken as the characteristic scales. Furthermore, the pressure is scaled by $(12\eta_1 D_f^2)/(b^2 t_f)$. Thus, the dimensionless version of the governing equations (1)–(3) can be expressed as

$$\nabla \cdot \mathbf{u} = 0, \tag{5}$$

$$\nabla p = -\eta\mathbf{u} \tag{6}$$

$$\frac{\partial c}{\partial t} + \mathbf{u}\cdot\nabla c = \frac{1}{\mathrm{Pe}}\nabla^2 c. \tag{7}$$

In the context of our problem, dimensionless controlling parameters such as the Péclet number Pe (relative measure of advection and diffusion effects), and the viscosity A (dimensionless viscosity difference) are defined as

$$\mathrm{Pe} = \frac{D_f^2}{Dt_f}, \quad A = \frac{e^R - 1}{e^R + 1}.$$

The entire alternating injection procedure is carried out by sequentially injecting even amounts of the less viscous fluid, and the more viscous fluid, for n full cycles till the completion of the process at time $t = 1$. Each cycle contains two alternating injection stages, whose injection duration lasts Δt to yield the same total amount of injection, e.g., $n\Delta t = 0.5$, for each fluid. These three dimensionless parameters (Pe, A, Δt) will be used in the rest of this work to investigate how the alternating injection process and viscous fingering affect fluid mixing in radial Hele-Shaw flows.

B. Numerical scheme

The numerical methods we employ in this work are similar to the ones developed in Refs. [14,23,25–28], in which the governing equations have been conveniently recast into the well-known stream-function–vorticity (ϕ-ω) formulation, yielding

$$u_x = \frac{\partial \phi}{\partial y}, \quad u_y = -\frac{\partial \phi}{\partial x}, \tag{8}$$

$$\nabla^2 \phi = -\omega, \tag{9}$$

where the vorticity is related to the gradients in concentration as

$$\omega = -R\left(u_x \frac{\partial c}{\partial y} - u_y \frac{\partial c}{\partial x}\right).$$

In the present radial injection Hele-Shaw flow, the rotational component of the velocity is smooth and can be obtained numerically with high accuracy, while the potential part of the outward velocity induced by injection is related to a flow singularity at the source origin. The flow singularity makes accurate computations more difficult near this central location. To avoid numerical instabilities near the source, we smooth out the point source by distributing its strength in a Gaussian way over the initially circular core region, i.e., $r \leqslant D_c$, where r and D_c denote the dimensionless radial distance away from the point source and the dimensionless core diameter ($D_c = D_0/D_f$), respectively. Scaled by a characteristic injection rate ${D_f}^2/t_f$, the magnitude of the dimensionless potential radial velocity satisfying these requirements can be expressed as [23,25,27]

$$\mathbf{u}_{\mathrm{pot}} = -\frac{Q}{2\pi r}\left[1 - \exp\left(-4r^2/{D_c}^2\right)\right]\hat{\mathbf{r}}, \tag{10}$$

where $\hat{\mathbf{r}}$ represents the unit vector along the radial direction. The dimensionless injection strength Q in the above expression takes the form $Q = \pi(1 - {D_c}^2)/4$.

The simulations are performed till the completion time at $t = 1$ in a square computational domain with length of 3/2, which is sufficiently large to contain the injected fluid inside. A circular core with a diameter of $D_c = 0.15$ initially filled with the less viscous fluid is placed at the center of

the domain to start the injection process. To proceed with the alternating injection, fluids inside the circular core will be swapped when the injected fluid is changed. A small magnitude random noise is applied to the positions of 0.5 concentration along the core circumference, i.e., $r = 0.075$, at the beginning of each alternating injection stage to break the unphysical, artificial symmetric shape of the fingering patterns. Since the flux across the boundary is prescribed by the potential part, the rotational components of velocity are confined in the computational domain. As a result, a vanishing stream-function condition can be applied on the boundary. Moreover, since the computational domain is large enough to accommodate the injected fluid, the concentration is uniform on the boundaries, so that vanishing concentration gradient is used. By incorporating these ingredients, the boundary conditions are prescribed as follows:

$$x = \pm 3/4 : \phi = 0, \quad \frac{\partial c}{\partial x} = 0, \tag{11}$$

$$y = \pm 3/4 : \ \phi = 0, \quad \frac{\partial c}{\partial y} = 0. \tag{12}$$

To reproduce the extremely fine structures of the fluid fingers, a highly accurate pseudospectral method is employed. For implementation of the pseudospectral method, the actual boundary conditions applied in the numerical code are $\partial\phi/\partial x = 0$ at $x = \pm 3/4$. However, at the present situation, where no gradient of the concentration is generated on the boundaries, the above conditions automatically lead to $\phi = 0$. Both c, and ϕ are expanded in a cosine series in the x direction. In the y direction, discretization is accomplished by sixth-order compact finite differences. Time integration for the phase variable is fully explicit and utilizes a third-order Runge-Kutta procedure. The evaluation of the nonlinearity at each time level is performed in a pseudospectral manner. Simulations that used a similar approach [23,27] have been validated by comparing the growth rates with the respective values obtained from linear stability theory. For a more detailed account of these numerical schemes and their validations, the reader is referred to Refs. [14,23,26–28].

Here, we briefly comment on the fact that the two Cartesian coordinates are treated differently in our numerical simulations. Considering the circular geometry of the physical problem under study, a polar coordinate system would obviously seem more appropriate. Nevertheless, this is not always the case if the numerical accuracy is a major concern. In order to successfully produce the extremely fine and intricate structures emerging in the miscible fingering problems, highly accurate numerical schemes are essential, e.g., the pseudospectral method associated with high-order compact finite-difference schemes. In practice, the implementation of these high-order schemes impose serious limitations on a polar coordinate description, but perform much better in a uniform Cartesian grid. This is the reason why a rectangular coordinate system is adopted to describe the current injection flow situation. A detailed discussion regarding the justifications for the use of the rectangular coordinate system for similar radial Hele-Shaw flows is provided in Ref. [29].

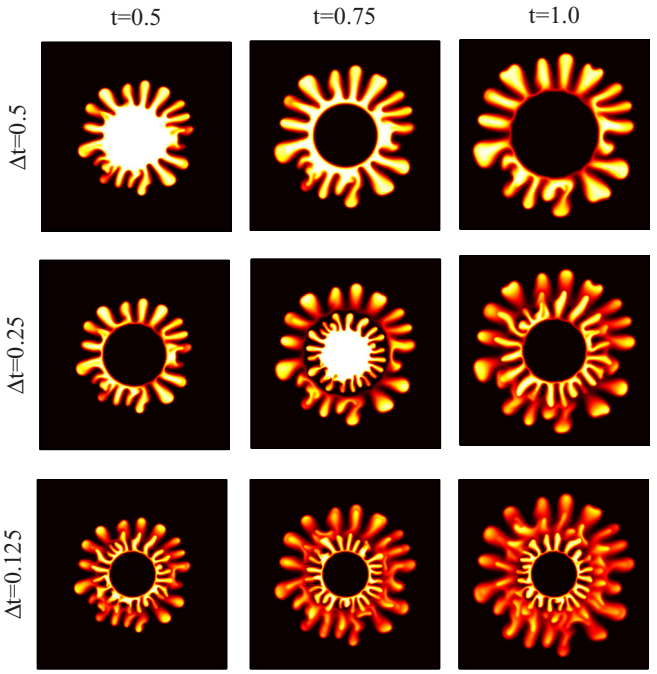

FIG. 1. (Color online) Evolution of concentration images for Péclet number Pe = 3000, viscosity contrast $A = 0.922$, and different alternating injection intervals $\Delta t = 0.5$ (top row), 0.25 (middle row) and 0,125 (bottom row), taken at times $t = 0.5$ (left column), 0.75 (middle column), and 1 (right column).

III. RESULTS AND DISCUSSION

A. Fingering and flow patterns

Shown in Fig. 1 are concentration images for a representative series of numerical simulations considering Pe = 3000 and $A = 0.922$, for alternating injection time intervals $\Delta t = 0.125$, 0.25, and 0.5, taken at times $t = 0.5$, 0.75, and 1. First, let us examine the situation in which $\Delta t = 0.5$ (top row of Fig. 1), where we have just one cycle of alternating injection ($n = 1$), and the injection of the less viscous fluid occurs for $0 \leqslant t \leqslant 0.5$. Under such circumstances, and at time $t = 0.5$, the inner region of the simulated domain is fully occupied by the less viscous fluid (clear fluid). In this first stage of injection, a typical miscible fingering pattern is obtained, where some fingers merge and others tend to split at their tips. Then, in a second stage of injection, the more viscous fluid (dark fluid) is introduced, characterizing the expansion of a stable circular blob when $0.5 < t \leqslant 1.0$. The development of such a stable circular structure should not be surprising, since here a more viscous fluid is pushing a less viscous one, establishing a stable displacement in the Saffman-Taylor problem. On the other hand, one can see that the less viscous fingers formed during the previous injection stage keep evolving. However, due to the lack of a continuous supply of less viscous fluid during this outward expansion, one notices that diffusion effects take place within the less viscous fluid. As compared to the case of the sole injection of the less viscous fluid up until $t = 0.5$, a better mixing performance is achieved by the injection of the additional volume of the more viscous fluid for $0.5 < t \leqslant 1.0$. These basic observations indicate that the alternating injection procedure, i.e., initial

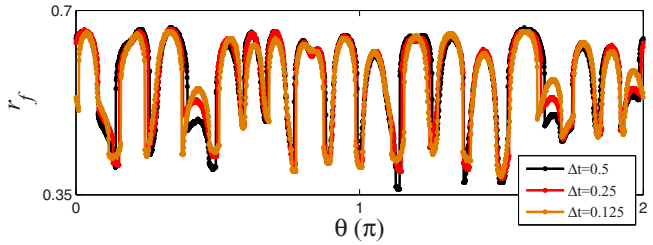

FIG. 2. (Color online) Interfacial profiles, represented by concentration contours with $c = 0.1$ at $t = 1$, for $A = 0.922$, and $\mathrm{Pe} = 3000$, whose correspondent images are shown in the right column of Fig. 1. Here the dimensionless radial position of the outermost interfacial profile r_f is plotted as a function of the polar angle θ. Despite the active interactions amongst the fingering structures, changes in the alternating injection interval Δt do not significantly alter the ultimate shape of the peripheral fingering patterns.

injection of the less viscous fluid followed by the injection of the more viscous one, improves the fluid mixing performance by effectively increasing the total diffusive interfacial length. It is worth pointing out that these radial flow findings are in line with similar results obtained in Ref. [17] for miscible flow in rectangular Hele-Shaw cells.

Now we turn our attention to the cases in which smaller alternating injection time intervals Δt are used, involving a larger number (n) of injection cycles. We begin by analyzing the case in which $\Delta t = 0.25$ and $n = 2$ as depicted in the middle row of Fig. 1. By increasing the number of alternating injection cycles, more fluid-fluid interfaces are generated, which tends to enhance fluid diffusive mixing. It is also evident that the multiple alternating injection cycles form fluid layers of the less viscous fluids that are separated by the more viscous fluid, triggering the emergence of fingering instabilities. While the outermost fingering layer of the less viscous fluid advances slowly, the less viscous fingers in the inner layer expand much faster, breaking through the more viscous fluid layer. These inner fingers eventually reach the roots of outer fingers, leading to the development of salient fingering interactions, where the occurrence of finger interpenetration and finger merging is detected. All these factors combined conspire to improve fluid mixing.

For even smaller alternating injection intervals, as in the case where $\Delta t = 0.125$ and $n = 4$ (illustrated in the bottom row of Fig. 1), the fluid layers are thinner and visually striking fingering patterns arise, so that an improved fluid mixing performance is obtained. This can be easily verified by inspecting the final concentration images taken at time $t = 1$, shown in the right column of Fig. 1.

It is worthwhile to note that, regardless the values of the injection intervals Δt, the resulting outermost fingering interface patterns look very similar to one another. This is more clearly illustrated in Fig. 2, whose interfacial profiles are represented by the concentration contour with $c = 0.1$. There, it can be observed that the overall shapes of the peripheral interfacial profiles taken for $t = 1$ are almost identical. Still, there are some small differences: for instance, for the interface located farther away from the origin, in particular for the fingertips of the faster advancing fingers, the interfacial profile

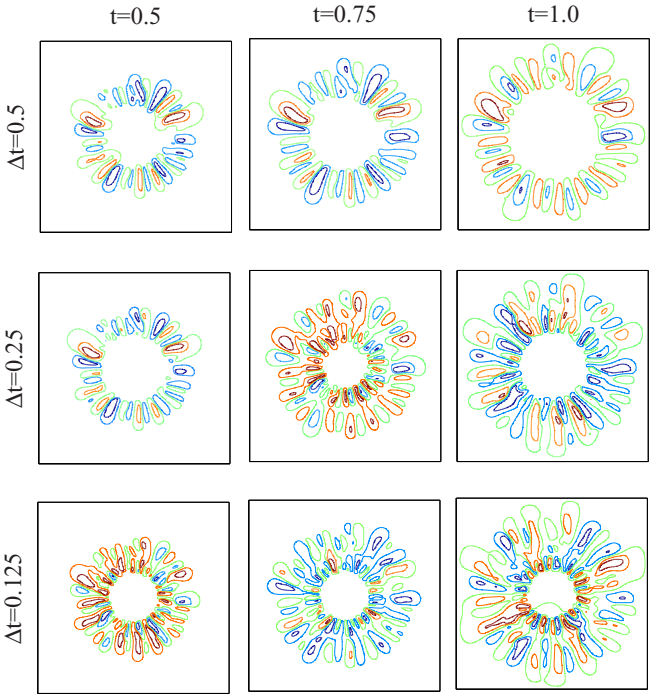

FIG. 3. (Color online) Evolution of the rotational component of the streamlines, corresponding to the concentration images depicted in Fig. 1.

is slightly ahead for larger injection intervals. In contrast, for the interface closer to the origin, e.g., the roots of the fingers or tips of slower advancing fingers evolve in an opposite manner, where the interfacial profiles associated to smaller injection intervals are ahead. These distinct behaviors can be understood by the local distribution of vortices generated by fingering interactions, as discussed in the following paragraph.

To understand the dynamics of fingering interactions, the rotational component of the streamlines for the cases presented in Fig. 1 are shown in Fig. 3. In the context of miscible viscous fingering events, it is well known that each individual finger is formed by a pair of counter-rotating vortices [23]. The strength of such vortex pairs is measured by the local density distribution of streamlines. Keeping this in mind, we examine the situation in which $\Delta t = 0.5$ (top row of Fig. 3). For the first injection stage ($t \leqslant 0.5$) one observes the uprising of numerous vortex pairs, which in turn corresponds to the initial formation of the various fingers. At the second injection stage, when the more viscous fluid is injected ($0.5 < t \leqslant 1$), these vortex pairs are moved in the outward direction. Since the injection at this second stage corresponds to a stable Saffman-Taylor situation, the strength of the vortex pairs is weakened, and the pairs just suffer a relatively mild stretching.

If the injection interval is reduced to $\Delta t = 0.25$ (middle row of Fig. 3), the fingering formation up to time $t = 0.5$ is similar to the previous case for which $\Delta t = 0.5$, since it has gone through just a full cycle of injection. This explains the resemblance of the streamline patterns at $t = 0.5$ for these two cases ($\Delta t = 0.5$ and $\Delta t = 0.25$). Notice that the strength of the vortex pairs is reduced for $\Delta t = 0.25$ because only a half amount of the less viscous fluid has been injected. Afterwards, injection of the less viscous fluid is resumed ($0.5 < t \leqslant 0.75$)

to generate an additional inner layer of vortex pairs. These inner vortex pairs are of larger magnitude, and expand faster than those associated to the outer fingers. As a consequence, these two layers of vortex pairs interact very intensively. By inspecting the streamlines at $t = 0.75$ one verifies the formation of two distinguishable layers of vortex pairs, in which the strength of the inner layer vortex pair is much stronger. The vortex pairs of these two distinct layers are not entirely separated, and can merge. These vortex pairs' merging phenomena continue for $0.75 < t \leqslant 1$, when the injection is alternated again, to allow insertion of the more viscous fluid. In this case, closely located streamlines are further stretched, and contain multiple vortices.

The phenomena described in the two previous paragraphs are even more evident for a smaller injection interval, e.g., for $\Delta t = 0.125$ (bottom row of Fig. 3). Stretched streamlines containing multiple vortices are fully formed at $t = 0.5$, when two full cycles of alternating injection have been completed. This trend, associated with active vortex merging, keeps developing till the end of injection process at time $t = 1$, when the resulting streamline patterns are quite complicated. These complex patterns are related to enhanced convective mixing effects between the staggered fluid layers of the two fluids, as exemplified in the bottom row of Fig. 1. In addition, the significant vortex interactions in the innermost layer also explains the faster advance of the interfacial profile closer to the origin for a smaller injection interval, as identified in Fig. 2. In summary, the material presented in Figs. 1–3 supports the idea that, for radial Hele-Shaw flows, smaller alternating injection intervals Δt do favor greater mixing in the bulk, while keeping the shape of the outermost interface profile nearly unchanged.

From the results and discussions presented so far in this section, one can list two main causes for the enhanced mixing obtained in radial Hele-Shaw flows through an alternating injection method: (i) the formation of a longer diffusive interface, and (ii) the existence of conspicuous fingering interactions. Nevertheless, with respect to the influence of the Péclet number Pe on mixing, these two factors seem to be somehow conflicting. On one hand, smaller values of Pe do improve diffusive mixing through the formation of longer diffuse interfaces. But, on the other hand, smaller Péclet numbers also weaken the fingering interactions, which are preferred under stronger convective conditions. In order to investigate these two distinct roles played by the Péclet number, in Fig. 4 we present representative simulations considering that $\Delta t = 0.1$ and $t = 1$, for three increasingly larger values of the Péclet number: 1000, 3000, and 6000. This is done for two values of the viscosity contrast A: 0 and 0.848. The series for viscosity matched fluids $A = 0$ (top row of Fig. 4) illustrates the purely diffusive cases, while the sequence for $A = 0.848$ (bottom row of Fig. 4) represents the conditions associated with strong fingering interactions.

When $A = 0$, the fluids have equal viscosities (stable Saffman-Taylor situation), so that fingers are not formed. Instead, the alternating layers of viscous fluid 1 (clear fluid) and of fluid 2 (dark fluid) evolve as multiple, concentric circular layers. By examining the top row of Fig. 4 one clearly sees that these circular annuli are more strongly diffused for Pe = 1000,

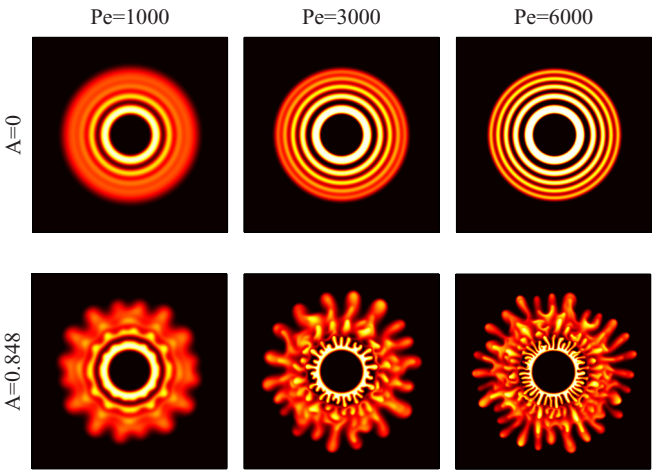

FIG. 4. (Color online) Concentration images obtained for $\Delta t = 0.1$ at time $t = 1$, $A = 0$ (top row), $A = 0.848$ (bottom row), and for three values of the Péclet number: 1000 (left column), 3000 (middle column), and 6000 (right column).

and much better preserved for Pe = 6000. As expected, fluid mixing is more effective for lower values of the Péclet number.

However, things are not that straightforward for the high viscosity contrast case ($A = 0.848$), when significant fingering formation is present. In this situation a nontrivial coupling between A and Pe takes place. As depicted in the bottom row of Fig. 4, the occurrence of fingering is evidently restrained for lower values of Pe. In fact, interfacial expansion is more evenly distributed for Pe = 1000. The strong diffusive effects associated with this low value of Pe lead to significant mixing, especially at more external fluid layers that have been generated by the earlier injection cycles. Nonetheless, higher values of the Péclet number (e.g., Pe = 6000) lead to intense fingering interactions also resulting in strong and complex dispersive mixing. This behavior is in stark contrast with the case for $A = 0$ and Pe = 6000 where the integrity of the multiple circular layers of fluids is much better retained. In the following section we will show that this dispersive mixing for higher Péclet number is slightly more efficient than the diffusive mixing under lower Pe. As we will see, the interplay of diffusive and convective-dispersive mixing, which depends on the coupling between A, Pe and Δt, plays a central role in determining the effectiveness of the mixing process.

B. Quantitative measures

In the previous section, we have qualitatively verified that the mixing performance can be boosted by employing an alternating injection scheme, associated with smaller injection intervals. It turns out that the mixing efficiency can be more quantitatively measured by the variance of the concentration distribution which is calculated by [15,17,30]

$$\sigma^2 = \sum_i \frac{A_i (c_i - c_m)^2}{A_0}. \tag{13}$$

Here, c_m is the instantaneous mean concentration of the entire computational domain excluding the core area, denoted as A_0. A_i and c_i are the area of every discretized mesh, and the local

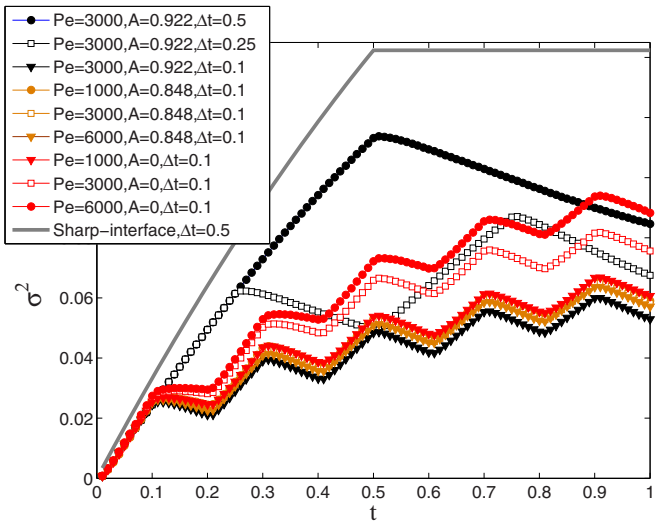

FIG. 5. (Color online) Time evolution of the concentration variance σ^2 for several values of the control parameters Pe, A, and Δt. Lower values of the variance imply enhanced mixing efficiency.

concentration in the mesh, respectively. A smaller value of the variance indicates better fluid mixing, so that in a perfectly mixed state $\sigma^2 = 0$. The temporal mean concentration can be written as $c_m(t) = Q_1/A_0$, where $Q_1(t)$ is the instantaneous injected area of the less viscous fluid 1. Under these conditions, injection of the fluid 1 always increases the variance, while the variance remains constant if injection is switched to the fluid 2.

For the sake of clarity, at this point we briefly discuss a special condition associated with stable injection of an immiscible fluid, e.g., sharp interface without diffusion. In such circumstances, the variance is given by $\sigma^2(t) = Q_1(A_0 - Q_1)/A_0^2$. A representative case, showing as the variance evolves with time for $\Delta t = 0.5$, is plotted in Fig. 5 (solid curve). In this case, the concentration variance presents a rapid increase during the first injection stage of fluid 1 for $t \leqslant 0.5$, then reaches a maximum value ($\sigma_m^2 = 0.1424$). Subsequently, when ($0.5 < t \leqslant 1$), the variance remains constant when the injection is alternated to fluid 2. By the way, under this immiscible sharp interface condition, the maximum variance at the completion time $t = 1$ is kept unchanged, regardless the injection time interval. So, it can be used as a reference value to determine the enhancement of mixing.

We proceed with our examination of Fig. 5, and now focus on the impact of the alternating injection interval Δt on the time evolution behavior of σ^2. First, we consider the situations in which $\Delta t = 0.5, 0.25$, and 0.1, for Pe $= 3000$ and $A = 0.922$. For the miscible and unstable injection scenario, one readily observes that the curve for $\Delta t = 0.5$ significantly deviates from the reference immiscible sharp interface curve. In fact, the variance growth during the unstable injection interval of the less viscous fluids at the first stage, i.e., $t \leqslant 0.5$, is considerably smaller for the present condition where $\Delta t = 0.5$. In addition, one can see that the variance decays even during the second stable injection stage of the more viscous fluid, i.e., when $0.5 < t \leqslant 1$. We have verified that the variance at the completion time ($t = 1$) is reduced more than 35% as compared to the reference case. These more quantitative findings further support the idea that alternating injection is a suitable method to achieve enhanced mixing in radial flows.

The behaviors described above can be more physically explained by considering the contribution of two key factors mentioned in Sec. III A: diffusive mixing and convective fingering interactions. The decrease of the variance growth rate in the first unstable injection stage can be mainly attributed to the fingering interactions, when vigorous fingering instabilities take place. On the other hand, the decline of the variance during the stable injection is mostly related to diffusive effects, since no extra fingers evolve at this second stage. If the alternating injection interval is reduced to $\Delta t = 0.25$ in Fig. 5, the evolution of the variance in the first full cycle, i.e., $0 \leqslant t \leqslant 0.5$, is somewhat similar to the previous case in which $\Delta t = 0.5$, except for the fact that the time periods for the two stages are shorter. Despite this, both the variance growth rate of the unstable injection and the variance decline of the stable injection are more significant in the second cycle ($0.5 < t \leqslant 1$). Similar dynamical responses are found if the injection interval is reduced further to $\Delta t = 0.1$. All these data offer quantitative indications that a better mixing performance is achieved through the utilization of shorter Δt, i.e., via the employment of more alternating injection cycles.

To evaluate more perceptibly the influence of the Péclet number, whose antagonistic roles regarding mixing have been qualitatively discussed in the previous section, we plot the temporal evolution of the variance for the pattern-forming images illustrated in Fig. 4, whose related parameters are also presented in Fig. 5: Pe $= 1000$, 3000, and 6000; $A = 0$, and 0.848, and $\Delta t = 0.1$. For the stable Saffman-Taylor cases in which $A = 0$, where the major contributor to mixing is fluid diffusion, smaller Péclet numbers always lead to lower values of variance. The prevalence of the diffusive effects can be clearly verified from the almost identical growth rates, i.e., the curves evolve in an almost parallel fashion during the injection stage of fluid 1 for all cycles, in spite of the value of the Péclet number. On the contrary, the decrease of the variance during the injection stages of fluid 2 is more intense for lower values of the Péclet number. For instance, the variance for the case in which Pe $= 6000$ almost remains constant during the injection stage of fluid 2 in the first cycle, i.e., $0.1 < t < 0.2$, which indicates little influence of diffusion. The variance drops off more evidently at this stage for the case in which Pe $= 1000$. Consequently, at these diffusion dominated stages larger decreases in the variance for cases of smaller Péclet number accumulate throughout all the injection cycles, and results in a greater mixing performance at $t = 1$, as shown in Fig. 5.

The situation for the unstable Saffman-Taylor cases in Fig. 5 for which $A = 0.848$ is a bit different. Although the concentration images shown in the bottom row of Fig. 4 are qualitatively distinct, the influence of the Péclet number to fluid mixing is not quantitatively significant. This is supported by the fact that in Fig. 5 the three variance curves for Pe $= 1000$, 3000, and 6000, $A = 0.848$ and $\Delta t = 0.1$ practically overlap. The minor differences among these curves point to a compromise between the strong dispersion effects induced by vigorous fingering interactions under high Péclet number conditions, and strong diffusion in the cases of low

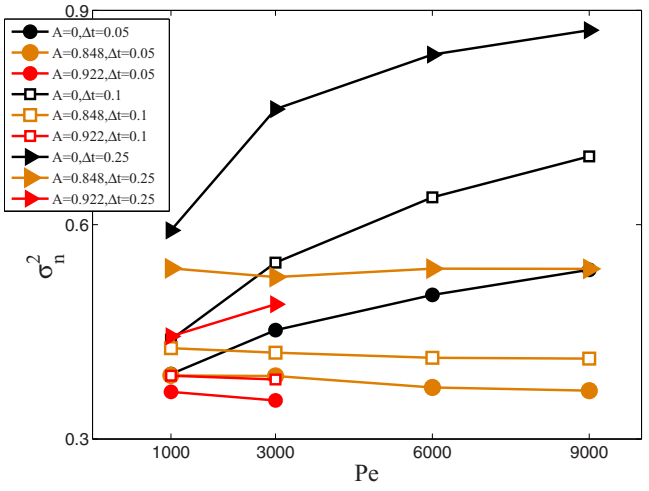

FIG. 6. (Color online) Behavior of the normalized variance σ_n^2 as the Péclet number Pe is changed, for $t = 1$, and several values of the control parameters A and Δt. Note: the cases for $A = 0.922$ and Pe $\geqslant$ 6000 are numerically unstable, so they are not presented.

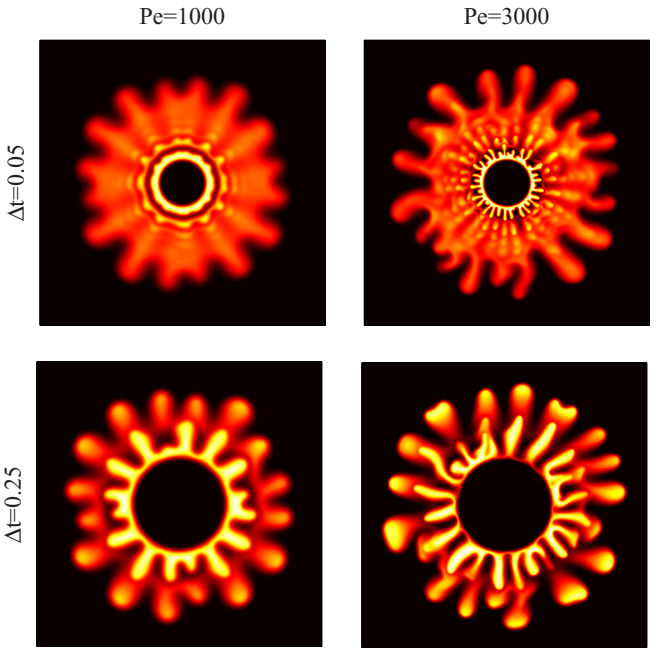

FIG. 7. (Color online) Fingering patterns for $A = 0.922$ at $t = 1$, $\Delta t = 0.05$ (top row), $\Delta t = 0.25$ (bottom row), Pe = 1000 (left column), and Pe = 3000 (left column).

Péclet number. Despite these observations, by inspecting Fig. 5 one can see a slight better mixing performance for the higher Péclet number situation (Pe = 6000). Finally, from Fig. 5 (see the cases $A = 0$, 0.848, and 0.922 for Pe = 3000 and $\Delta t = 0.1$) one can also tell that better mixing performance can always be achieved by larger viscosity contrast, due to the occurrence of more intense fingering interactions.

We continue our discussion by studying Fig. 6, which plots the normalized variance $\sigma_n^2 = \sigma^2/\sigma_m^2$ in terms of the Péclet number Pe at the completion time $t = 1$, for several combinations of the control parameters A, and Δt. The general trends of better mixing performances for shorter alternating injection interval Δt, and for higher viscosity contrast A are confirmed by the data shown in Fig. 6. However, the mixing efficiency related to the action of the Péclet number depends on the coupling with fingering interactions. For stable cases in which $A = 0$, stronger diffusion at lower Péclet number always leads to a better mixing performance. However, this is not true when fingering instabilities are triggered for sufficiently large viscosity contrasts, e.g., $A = 0.848$ and 0.922. For shorter alternating injection intervals ($\Delta t = 0.05$ and 0.1), the normalized variance decreases slightly for higher Péclet number, which is in line with the discussion we had earlier. On the other hand, this monotonic trend is not followed for longer alternating intervals, e.g., for $\Delta \geqslant 0.25$.

The nontrivial competition between diffusion and fingering interactions can be better visualized in Fig. 7, which shows the concentration images of typical cases for $A = 0.922$ at $t = 1$. For a shorter alternating injection interval ($\Delta t = 0.05$), the fluid layers formed in different cycles of fluid injection are extremely thin. Consequently, diffusive effects in the case of Pe = 1000 and fingering interactions for the case of Pe = 3000 are both very significant, and smear off the concentration variation. Most of the regions present significant diffusion or dispersion to form circular mixing cores in both cases. The slightly better overall mixing performance for higher Pe = 3000 indicates extremely intense fingering interactions among the numerous thin layers of the injected fluid.

A completely different scenario is obtained in Fig. 7 for a longer injection time interval $\Delta t = 0.25$, where the concentration images reveal very different types of patterns, in which the widths of the staggered fluid layers are considerably thicker. These thicker fluid layers allow more independent growth for the long fingers, before they start to interact with each other. Therefore, when $\Delta t = 0.25$ most of the inner fingers penetrate into the outer layer, rather than expanding as a circular mixing core, as happened in the case for $\Delta t = 0.05$. This absence of active fingering interactions is consistent with the poorer mixing performance for higher Péclet numbers.

The results extracted from the data displayed in Figs. 5–7 indicate, now more quantitatively, that the action of the Péclet number is not monotonic, but couples with A and Δt. Diffusive effects are the dominant mechanism for fluid mixing under situations of weak fingering instability. In this case, lower Péclet numbers tend to enhance mixing efficiency. On the other hand, if intense fingering is triggered at larger viscosity contrasts, the results do not follow the same trend. For cases associated with shorter alternating injection intervals, fluid mixing performance is enhanced for higher Péclet numbers because of prominent interactions between the fingers generated by different injection cycles. Nevertheless, mixing efficiency is found to be unaltered or even decreased for conditions of sufficiently high viscosity contrast at longer alternating injection intervals, e.g., $A = 0.922$ and $\Delta t \geqslant 0.1$. This somewhat unexpected behavior can be mainly attributed to the formation of the long highly branched fingers induced by sufficiently high viscosity contrast. The emerging fingers tend to penetrate deeper toward the surrounding fluid under higher viscosity contrast, so that longer fingers evolve after a period of time, as recently revealed experimentally in Ref. [31]. If the injecting time interval is also long enough for the emergence

of these long fingers, the fluid interactions will be constrained to occur within these few long fingers, as shown on the bottom row in Fig. 7. This constrained fingering interaction will be more significantly coupled under more unstable fingering conditions associated to a higher Péclet number. As a result, the overall mixing efficiency will not be improved, and may even be reduced if both the viscosity contrast and injecting time interval are sufficiently large.

IV. CONCLUDING REMARKS

In this work, intensive numerical simulations have been used to study enhanced mixing induced by viscous fingering and alternating injection in confined radial Hele-Shaw flows. As in the rectangular flow case studied by Jha *et al.* [15–17], we have verified that the alternating injection method significantly improves the mixing performance in radial geometry. An inspection of the complex concentration images for the mixing patterns reveals the following general dynamic scenario: on one hand, alternating injection generates multiple fluid layers, and effectively increases the interfacial contact area between the fluids, leading to more diffusive mixing. On the other hand, the thin fluid layers produced during different injection cycles result in strong fingering interactions, which greatly enhances dispersive fluid mixing.

A more quantitative assessment of the problem was provided by the concept of concentration variance, which quantifies the mixing efficiency. With the help of this useful statistical quantity, we could better substantiate our qualitative findings regarding fluid mixing. First, we verified that the overall mixing performance is indeed considerably improved by the shortening of the alternating injection intervals.

The interplay of the alternating injection interval Δt with other key control parameters of the system (namely, the Péclet number Pe, and the viscosity contrast A) have also been investigated. As expected, we have found that larger A triggers more vigorous fingering instability, leading to a better mixing performance.

However, the role played by Pe is a bit more subtle: for the cases in which fingering interactions are intense, e.g., large A associated with shorter Δt, a higher Péclet number result in a better mixing. Differently, a lower Péclet number performs a better job for mixing either for diffusion-dominated conditions without active fingering instability, or when fingering interactions are less intense, for sufficiently low A. This also happens for sufficiently high A, but associated to longer alternating injection intervals.

ACKNOWLEDGMENTS

J.A.M. thanks CNPq and FACEPE (through PRONEM Project No. APQ-1415-1.05/10) for financial support. C.-Y.C. thanks the Ministry of Science and Technology, the Republic of China (Taiwan) for financial support through Grant No. MOST 101-2221-E-009-033-MY3.

[1] P. G. Saffman and G. I. Taylor, Proc. R. Soc. London Ser. A **245**, 312 (1958).
[2] G. M. Homsy, Annu. Rev. Fluid Mech. **19**, 271 (1987).
[3] K. V. McCloud and J. V. Maher, Phys. Rep. **260**, 139 (1995).
[4] R. Govindarajan and K. C. Sahu, Annu. Rev. Fluid Mech. **46**, 331 (2014).
[5] L. Paterson, J. Fluid Mech. **113**, 513 (1981).
[6] O. Praud and H. L. Swinney, Phys. Rev. E **72**, 011406 (2005).
[7] A. Riaz, C. Pankiewitz, and E. Meiburg, Phys. Fluids **16**, 3592 (2004).
[8] S. B. Gorell and G. M. Homsy, SIAM J. Appl. Math. **43**, 79 (1983); J. P. Stokes, D. A. Weitz, J. P. Gollub, A. Dougherty, M. O. Robbins, P. M. Chaikin, and H. M. Lindsay, Phys. Rev. Lett. **57**, 1718 (1986).
[9] Y. K. Suh and S. Kang, Micromachines **1**, 82 (2010).
[10] S. Li, J. S. Lowengrub, J. Fontana, and P. Palffy-Muhoray, Phys. Rev. Lett. **102**, 174501 (2009).
[11] C.-Y. Chen, C.-W. Huang, L.-C. Wang, and J. A. Miranda, Phys. Rev. E **82**, 056308 (2010).
[12] E. O. Dias and J. A. Miranda, Phys. Rev. E **81**, 016312 (2010).
[13] E. O. Dias, E. Alvarez-Lacalle, M. S. Carvalho, and J. A. Miranda, Phys. Rev. Lett. **109**, 144502 (2012).
[14] Y.-S. Huang and C.-Y. Chen, Comput. Mech. **55**, 407 (2015).
[15] B. Jha, L. Cueto-Felgueroso, and R. Juanes, Phys. Rev. Lett. **106**, 194502 (2011).
[16] B. Jha, L. Cueto-Felgueroso, and R. Juanes, Phys. Rev. E **84**, 066312 (2011).
[17] B. Jha, L. Cueto-Felgueroso, and R. Juanes, Phys. Rev. Lett. **111**, 144501 (2013).
[18] C.-Y. Chen and S.-W. Wang, Fluid Dyn. Res. **30**, 315 (2002).
[19] C.-Y. Chen and S.-W. Wang, Int. J. Numer. Meth. Heat Fluid Flow **11**, 761 (2001).
[20] A. De Wit, Y. Bertho, and M. Martin, Phys. Fluids **17**, 054114 (2005).
[21] M. Mishra, M. Martin, and A. De Wit, Phys. Rev. E **78**, 066306 (2008).
[22] Q. Yuan and J. Azaiez, Chem. Eng. Sci. **109**, 136 (2014).
[23] C.-Y. Chen and E. Meiburg, J. Fluid Mech. **371**, 233 (1998).
[24] C. T. Tang and G. M. Homsy, Phys. Fluids **31**, 1330 (1988).
[25] C.-Y. Chen, C.-W. Huang, H. Gadêlha, and J. A. Miranda, Phys. Rev. E **78**, 016306 (2008).
[26] C.-Y. Chen, Y.-S. Huang, and J. A. Miranda, Phys. Rev. E **84**, 046302 (2011).
[27] E. Meiburg and C.-Y. Chen, SPE J. **5**, 129 (2000).
[28] C.-Y. Chen, Y.-S. Huang, and J. A. Miranda, Phys. Rev. E **89**, 053006 (2014).
[29] C.-Y. Chen, S.-Y. Wu, and J. A. Miranda, Phys. Rev. E **75**, 036310 (2007).
[30] S. B. Pope, in *Turbulent Flows* (Cambridge University Press, Cambridge, England, 2000), pp. 373–382.
[31] I. Bischofberger, R. Ramachandran, and S. R. Nagel, Nat. Commun. **5**, 5265 (2014).